Mitochondrial pyruvate carrier-mediated metabolism is dispensable for the classical activation of macrophages

Linyu Ran
Shanghai East Hospital, Tongji University
Song Zhang
Mayo Clinic https://orcid.org/0000-0002-9786-802X
Pei Zhao
Shanghai East Hospital, Tongji University
Jiaxing Sun
Shanghai East Hospital
Jiaqi Zhou
Chinese Academy of Sciences
Haiyun Gan
Chinese Academy of Sciences
Ryounghoon Jeon
Mayo Clinic
Qiang Li
Shanghai East Hospital, Tongji University
Joerg Herrmann
Mayo Clinic
Feilong Wang (wang_feilong@tongji.edu.cn)
Shanghai East Hospital, Tongji University

Article

Keywords: Mitochondrial pyruvate carrier, macrophages, LPS, inflammation, UK5099, hypoxia-induced factor 1α

Posted Date: March 10th, 2022

DOI: https://doi.org/10.21203/rs.3.rs-1413776/v1

Version of Record: A version of this preprint was published at Nature Metabolism on May 15th, 2023. See the published version at https://doi.org/10.1038/s42255-023-00800-3.

Abstract

Glycolysis is essential for the classical activation of macrophages (M1), but how glycolytic pathway metabolites engage in this process remains to be elucidated. Glycolysis culminates in the production of pyruvate, which can be transported into the mitochondria by the mitochondrial pyruvate carrier (MPC) followed by conversion to citrate and utilization in the TCA cycle. Alternatively, pyruvate can be metabolized to lactate under aerobic conditions, which had been considered to be the dominant route in the setting of classical macrophage activation. However, based on studies that used UK5099 as a MPC inhibitor and showed reduction in key inflammatory cytokines, the mitochondrial route has been considered to be of significance for M1 activation as well. Herein, using a genetic depletion model, we found that MPC is dispensable for metabolic reprogramming and the activation of M1. In addition, MPC depletion in myeloid cells has no impact on inflammatory responses and macrophage polarization toward M1 phenotype in the endotoxemia mice model. While UK5099 reaches maximal MPC inhibitory capacity at approximately 2–5μM, higher concentrations are required to inhibit inflammatory cytokine production in M1 and this is independent of MPC expression. Taken together, this study found MPC-mediated metabolism is dispensable for the classical activation of macrophages, and UK5099 inhibits inflammatory responses in M1 macrophages due to effects other than MPC inhibition.

Introduction

A growing body of knowledge demonstrates that the switch from oxidative phosphorylation to glycolysis plays a critical role in the inflammatory response of macrophages when stimulated with agents such as lipopolysaccharide (LPS) (classical activation) [1, 2, 3, 4]. Pyruvate, the last product of glycolysis, can be transferred into the mitochondria to fuel the tricarboxylic acid (TCA) cycle as citrate or it can be metabolized into lactate. The latter route, known as “aerobic glycolysis” or the “Warburg effect”, is considered to be the main final pathway in classically activated macrophages, allowing them to use (repurpose) the mitochondria for reactive oxygen species (ROS) generation rather than ATP production [5–7]. Consequently, ROS production stabilizes hypoxia induced factor 1α (HIF-1α) and promotes proinflammatory cytokines production [5–7]. The role of the alternative, mitochondrial route of pyruvate in this setting is less clear. The transport of pyruvate across the mitochondrial membrane is an active process, enabled by the mitochondrial pyruvate carrier (MPC) complex, which consists of two subunits: MPC1 and MPC2 [8, 9]. Interestingly, some studies found MPC-mediated metabolism to also be important for the activation of LPS-stimulated macrophages [10, 11, 12, 13]. In this setting, the theory has been that pyruvate transportation by MPC is required for acetyl-CoA production, histone acetylation, and epigenetic changes, which then facilitate inflammatory gene expression [10, 11]. However, these findings and interpretations are established based on pharmacological inhibition of MPC using α-cyano-β-(1-phenylindol-3-yl)-acrylate (UK5099) as such an inhibitor [10, 12, 13]. Therefore, closer examination of the MPC inhibitor UK5099 is warranted to clearly interpret the role of MPC in macrophage activation.

In this study, we confirmed that UK5099 reduces cytokine production of murine bone marrow derived macrophages (BMDMs) but found a clear dose dependency. UK5099 at high doses (100 μM) could

effectively suppress the inflammatory response of M1 macrophages, yet low doses of 2–10 μM failed to do so, despite being equally potent to reduce the transport of glucose-derived pyruvate into the mitochondria. Studies on BMDMs derived from a murine *Mpc* conditional knockout model confirmed that the anti-inflammatory effects of UK5099 were independent of MPC. Even more, *Mpc* depletion in general had no impact on metabolic reprogramming, ATP generation and inflammatory cytokines production in M1 macrophages. Of further significance, *Mpc* deficiency in myeloid cells had no impact on inflammatory responses and macrophage polarization toward M1 phenotype in the endotoxemia mice model. Based on these results, we conclude that MPC-mediated metabolism is dispensable for the classical activation of M1 macrophages and the anti-inflammatory effects of UK5099 seen at high concentrations relate to effects other than MPC inhibition.

Results

UK5099 suppresses inflammatory cytokines production by M1 macrophages in a concentration-dependent manner

UK5099 has been shown to be effective in reducing the inflammatory response of macrophages at concentrations of 50 to 200μM [10, 11, 12, 13]. Indeed, herein we found a clear dose-dependent effect of UK5099 on proinflammatory cytokine production above a threshold dose of 25μM without any impact on viability (Fig. 1a-1g). The anti-inflammatory action of UK5099 has been attributed to its function as a potent MPC inhibitor, leading to the reduction of pyruvate entry into the TCA cycle, which in turn decreases the incorporation of glucose-derived carbons into histone acetylation and epigenetic modulation of the inflammatory gene expression [10]. In this study, we found that UK5099 effectively inhibits MPC at concentrations under 5μM (Fig. 1h to 1n), but its suppressive effect on the inflammatory response of M1 macrophages is not related to either the suppressive effect on MPC (Fig. 1a to 1f), an increase in global histone acetylation (Fig. 1o and 1p) or impaired pyruvate transport into the mitochondria (Fig. 1h to 1n). UK5099 reduced the ratio of ^{13}C-glucose labeled TCA cycle metabolites starting at concentrations as low as 1μM. This inhibitory effect reached a plateau starting at 5μM without any further decrease in ^{13}C-labeling ratio at any higher concentrations (Fig. 1h to 1n).

Low concentrations of UK5099 slightly reduced basal OCR, while high concentrations slightly increased it (Fig. 2a). The intracellular ATP levels were not affected by different concentrations of UK5099 (Fig. 2b and 2c). UK5099, however, did reduce FCCP-stimulated OCR in a dose-dependent manner (Fig. 2a), and this trend matched the dose response of UK5099 in inhibiting inflammatory cytokine production (Fig. 1a-1f).

Since dysfunctional cellular respiration is known to be associated with impaired mitochondrial membrane potential [14, 15, 16, 17], we next tested the mitochondrial membrane potential of BMDMs after treatment with different concentrations of UK5099. As shown in Fig. 2d, 100μM UK5099, but not 2 and 10μM UK5099, significantly reduced mitochondrial membrane potential.

Impaired cellular respiration and mitochondrial membrane potential can lead to less accumulation of HIF-1α, which is critical for the activation of LPS-stimulated macrophages [5, 7, 18]. Indeed, 100μM UK5099, but not 2 and 10μM UK5099, strongly reduced HIF-1α protein levels in LPS stimulated WT macrophages (Fig. 2e) by modulation of HIF-1α stabilization rather than gene expression (Fig. 2f). Besides being important for the macrophage mediated inflammation [18], HIF-1α is an essential regulator of metabolic genes expression [19]. Indeed, herein high-dose UK5099 also reduced the expression of HIF-1α target glycolytic genes including hexokinase 2 (*Hk2*) and phosphofructokinase (*Pfk1*)(Fig. 2g and 2h).

Collectively, these data show that the suppressive effect of UK5099 on the inflammatory response of M1 macrophages requires high concentrations and correlates with impairment in oxidative phosphorylation, mitochondrial membrane potential, and HIF-1a levels, but seems to be unrelated to the suppressive effect on MPC.

UK5099 suppresses inflammatory responses of M1 macrophages independent of MPC expression

In order to address the role of MPC for the anti-inflammatory actions of UK5099, we generated *Mpc1*-floxed mice by CRISPR/dCas9/gRNA ($Mpc1^{fl/fl}$) (Fig. 3a). Breeding with Lyz2-Cre mice yielded mice with myeloid cell-specific deletion of *Mpc1* ($Mpc1^{-/-}$). As shown in Fig. 3b, *Mpc1* mRNA level in bone marrow derived macrophages (BMDMs) isolated from $Mpc1^{-/-}$ mice was dramatically reduced compared with those from $Mpc1^{fl/fl}$ mice, while *Mpc2* mRNA level remained unchanged (Fig. 3c). Neither MPC1 nor MPC2 protein was expressed in $Mpc1^{-/-}$ BMDMs (Fig. 3d and 3e), and both proteins are known to be indispensable to form a stable MPC complex [8, 9, 20].

Importantly, the suppressive effect of excess UK5099 on M1 macrophage pro-inflammatory cytokine production was not only seen in $Mpc1^{fl/fl}$ macrophages but also in macrophages devoid of MPC expression (Fig. 3f to 3l). RNA sequencing analysis confirmed that *Mpc* depletion had no impact on proinflammatory cytokine production contrary to UK5099 treatment (Fig. 3m-3o). Approximately 1400 genes including TNF-α, IL-6 and IL-12 were changed by UK5099 treatment in LPS stimulated BMDMs, while only 168 genes were altered by *Mpc* depletion (Fig. 3m to 3o). These gene expression patterns were similar between $Mpc1^{fl/fl}$ and $Mpc1^{-/-}$ BMDMs after UK5099 treatment (Fig. 3p). GO analysis indicated that UK5099 affects immune responses and cytokines production of LPS stimulated macrophages very broadly (Fig. 3q).

UK5099 at concentrations below 10μM slightly reduced but at 100μM UK5099 significantly decreased FCCP-stimulated OCR in both $Mpc1^{fl/fl}$ and $Mpc1^{-/-}$ BMDMs (Fig. 4a and 4b). UK5099 influences FCCP-stimulated maximum OCR more than basal OCR and ATP linked OCR, a portrait that is in line with OXPHOS inhibitors [21, 22, 23]. As shown in Fig. 4c to 4e, both *Mpc* depletion and UK5099 treatment effectively inhibited respiration driven by pyruvate. Of note, 2μM UK5099 reduced respiration to the similar levels to that of 100μM UK5099 and *Mpc* depletion, indicating that low concentrations of UK5099 are also able to effectively block the entry of pyruvate into TCA cycle. Therefore, the suppressive effect of

100 μM UK5099 on FCCP-stimulated respiration cannot be attributed to the blocked entry of pyruvate into the TCA cycle and OXPHOS, but instead may be due to inhibited oxidation of other off-target substrates.

We then evaluated the impact of UK5099 on respiration driven by glutamate, whose transportation into mitochondrial and subsequent metabolism is independent of MPC [14, 21, 22, 23,]. As expected, *Mpc* depletion had no impact on glutamate driven respiration (Fig. 4f to 4h). However, 100μM UK5099, but not 2 and 10μM UK5099, significantly reduced glutamate driven respiration in both $Mpc1^{fl/fl}$ and $Mpc1^{-/-}$ BMDMs, suggesting that high concentrations of UK5099 not only inhibit MPC but also suppress the utilization of glutamate. This effect is due to the inhibition of later steps of glutamate oxidation rather than less glutamate/glutamine fuel into TCA cycle, as high concentrations of UK5099 did not reduce ^{13}C-glutamine labeled TCA cycle metabolites (Fig. 4i to 4l) and glutamine consumption (Fig. 4m).

Lastly, high-dose UK5099 reduced HIF-1α expression as well as the expression of HIF-1α target glycolytic genes including hexokinase 2 (*Hk2*) and phosphofructokinase (*Pfk1*) and nonmetabolic genes such as adrenomedullin (*Adm*) and matrix metalloproteinases (*Mmps*) in both $Mpc1^{fl/fl}$ and $Mpc1^{-/-}$ macrophages (Fig. 4n and4o).

Taken together, these data confirm that MPC is not an essential requirement for anti-inflammatory and anti-metabolic effects of UK5099 on activated M1 macrophages.

Mpc **depletion reduces glucose fuel into TCA cycle but has no impact on metabolic reprogramming in LPS-stimulated macrophages**

In order to address the question if MPC-mediated transportation of glycolysis-derived pyruvate is required for the activation of macrophages by LPS in general, we conducted further studies. ^{13}C-glucose tracing showed that $Mpc1^{-/-}$ BMDMs had a significantly lower ratio of glucose-labeled TCA cycle metabolites compared with $Mpc1^{fl/fl}$ BMDMs (Fig. 5a to 5e), indicating effective reduction of glucose flux into the mitochondria. Interestingly, *Mpc* depletion resulted in increased ratio of ^{13}C-labeled pyruvate but had no impact on ^{13}C-labeled lactate, suggesting pyruvate was accumulated when the route to mitochondria was blocked (Fig. 5f to 5g). While the upstream TCA cycle metabolites citrate and succinate were reduced (Fig. 5h and 5i), downstream metabolites were similar between $Mpc1^{-/-}$ and $Mpc1^{fl/fl}$ BMDMs (Fig. 5j to 5k). There was also no difference in the total amounts of intracellular pyruvate and lactate (Fig. 5l and 5m). Importantly, *Mpc* depletion did not affect the metabolic reprogramming of macrophages stimulated by LPS, neither early increase in glycolysis (Fig. 6a), nor later decrease in oxidative phosphorylation (Fig. 6b). Likewise, glucose consumption and lactate production significantly increased after LPS stimulation to similar levels in $Mpc1^{-/-}$ and $Mpc1^{fl/fl}$ BMDMs (Fig. 6c and 6d). However, more pyruvate was secreted into the medium from $Mpc1^{-/-}$ cells (Fig. 6e). Importantly, there was no difference in ATP, ATP/ADP ratio, AMP/ATP ratio and energy chargy between $Mpc1^{-/-}$ and $Mpc1^{fl/fl}$ BMDMs before and after LPS stimulation (Fig. 6f-6i). *Mpc* depletion also had no impact on cell viability (Fig. 6j). The observation that oxidative phosphorylation and energy generation remained intact after *Mpc* depletion despite less pyruvate availability in the mitochondria to fuel the TCA cycle points to other compensatory

sources. Indeed, *Mpc1*$^{-/-}$ BMDMs consumed more glutamine (Fig. 6k) and had higher glutamine labeled TCA cycle metabolites compared with *Mpc1*$^{fl/fl}$ BMDMs (Fig. 6l to 6o), pointing to glutamine as a compensatory source and alternative substrate for oxidative phosphorylation.

Mpc **expression is dispensable for proinflammatory cytokines production in LPS-stimulated macrophages**

We next tested if *Mpc* depletion influences the inflammatory response of macrophages stimulated by LPS. Previous studies reported that MPC inhibition by UK5099 reduced the production of proinflammatory cytokines, including TNF-α, IL-6, IL-12 [10, 11, 12, 13]. Genetic *Mpc* depletion, as in this study, however, did not change the expression of these cytokines (Fig. 7a to 7c) or their secretion (Fig. 7d to 7f).

Previous studies indicated that the conversion of glycolysis-derived pyruvate to acetyl-CoA supports histone acetylation, which is deemed critical for inflammatory gene expression in M1 macrophages [10]. In the current study *Mpc* depletion in BMDMs did not decrease histone acetylation (Fig. 7g). Collectively, these data indicated that MPC mediated transportation of glucose-derived pyruvate into the mitochondria is not mandatory for histone acetylation or the activation of macrophages by LPS.

Mpc **depletion in myloid cells has no impact on inflammatory responses in vivo**

Although we demonstrated that MPC-mediated metabolism is dispensable for macrophage activation by LPS in vitro, current cell culture systems have major differences from real physiological conditions in terms of the levels and ingredients of the nutrition provided [24]. Therefore, we tested the role of MPC-mediated metabolism in inflammatory responses and macrophage polarization in vivo by peritoneally injection of LPS into *Mpc1*$^{-/-}$ and *Mpc1*$^{fl/fl}$ mice to induce an endotoxemia model. As shown in Fig. 8a-8f, the levels of both serum and peritoneal proinflmammtory cytokines, including TNF-α, IL-6 and IL-12, were comparable between *Mpc1*$^{-/-}$ and *Mpc1*$^{fl/fl}$ mice. Crossing floxed mice with Lyz2-Cre mice leads to conditional gene depletion in myeloid cells including peritoneal tissue-resident macrophages [25]. We then tested if *MPC* depletion affects the polarization of peritoneal macrophages toward M1 pheotype in vivo. As shown in Fig. 8g, there was no difference in the expression of CD86, which is a classical marker of macrophages in response to LPS stimulation, in peritoneal macrophages of *Mpc1*$^{fl/fl}$ and *Mpc1*$^{-/-}$ mice after LPS challenge. Therefore, *Mpc* depletion in myloid cells has no impact on inflammatory response and macrophage differentiation in vivo.

Discussion

Metabolic reprogramming of immune cells has been investigated intensively in recent years, but better understanding of how metabolism precisely controls immune reponses of these cells is still needed [1–5]. One aspect in question has been the role of MPC, mediating pyruvate transfer into the mitochondria. This question has been addressed in previous studies by the use of UK5099 as a specific MPC inhibitor. In this

study, we provide new data outling that the inhibitory effects of UK5099 on M1 macrophage activation are dose-dependent and MPC-independent. Indeed, in general MPC is not required for M1 macrophage activation *in vivo* and *in vitro*.

MPC-mediated metabolism is dispensable for the activation of LPS stimulated macrophages

After stimulation by LPS for 18 to 24 hours, one key metabolic signature of macrophages is the reduced oxygen consumption, increased mitochondrial membrane potential and reactive oxygen production generated by the electron transport chain [5, 7]. This process promotes HIF-1α stabilization to facilitate pro-inflammatory cytokines production [5, 7]. Interestingly, recent studies found that short term stimulation of BMDMs by LPS increases maximal respiratory capacity while maintaining an intact basal respiration, and that increased respiration is required for proinflammatory cytokine production [10, 11]. How glycolytic metabolites participate in this metabolic rewiring of LPS stimulated macrophages, however, remains unclear.

MPC-mediated metabolism is at the intersection of glycolysis, the TCA cycle and OXPHOS. Previous studies demonstrated that pharmacological inhibition of MPC by UK5099 attenuated glycolytic fueling of the mitochondria and the inflammatory response in LPS stimulated macrophages [10, 11, 12, 13]. Herein, however, we found that genetic depletion of *Mpc* has no effect on metabolic reprogramming and pro-inflammatory cytokine production in LPS stimulated macrophages. Although *Mpc* depletion substantially reduced the transportation of glycolysis-derived pyruvate into the TCA cycle, TCA cycle metabolites can be compensated for by other sources, such as glutamine, and therefore elevated maximal respiratory capacity is maintained to promote inflammatory responses. Indeed, previous studies indicated that the main source of accumulated TCA cycle metabolites in LPS stimulated macrophages was glutamine rather than glucose [6]. Collectively, our study supports the notion that the metabolic reprogramming of mitochondria is flexible and does not depend on MPC in LPS-activated macrophages.

Histone acetylation and macrophage activation

The role of histone acetylation in macrophage activation by LPS is controversial. Prior studies observed that LPS stimulation increases the incorporation of glucose-derived carbons into histone acetylation and that pharmacological inhibition of glycolysis by 2-DG or MPC by UK5099 reduces pro-inflammatory cytokines production. These observations led to the conclusion that the transportation of glycolysis-derived pyruvate into the mitochondria is essential for acetyl-CoA production, histone acetylation, and the activation of LPS stimulated macrophages [10, 11]. However, whether these inhibitory effects impact gobal levels of (rather than glucose incorporated) histone acetylation is unknown. Moreover, recent studies showed that genetic knockdown or depletion of ATP citrate lyase, which catalyzes citrate into acetyl-CoA in the cytoplasm, even increases cytokine production in LPS stimulated macrophages [26, 27]. Our study surprisingly found that both *Mpc* depletion and UK5099 treatment increased histone acetylation, even though intercellular citrate levels were reduced in both conditions. There are two

possible reasons for these data. First, cytosolic acetyl-CoA rather than mitochondrial acetyl-CoA is the substrate for histone acetylation. Although *Mpc* depletion resulted in less intercellular citrate, cytosolic acetyl-CoA can be compensated by accumulated pyruvate. Further, pyruvate can be catalyzed into acetate, and in turn to acetyl-CoA in cytosol [28]. Indeed, we found that *Mpc* depletion blocks the entry of pyruvate into the mitochondria and leads to more pyruvate release. Second, it is unknown if histone acetylation is strictly determined by the level of acetyl-CoA, which requires further investigation.

UK5099 inhibits the M1 macrophage inflammatory responses independent of MPC

Although the existence of MPC had long been anticipated, its molecular identity was not defined until 2012 [8, 9]. Since then, MPC-mediated metabolism has been investigated extensively [29–32]. One of the main agents used in these studies is UK5099, a potent inhibitor of MPC, thought originally invented as the analog of α-cyano-4-hydroxycinnamate (CHC) long before the discovery of MPC [33–34]. Studies found that it could reduce the entry of pyruvate into the mitochondria (with an IC_{50} of 50 nM in rat heart mitochondria) [33–34]. While wildly used, the specificity of UK5099 for MPC inhibition remains unknown. Studies have used a wide range of concentrations of UK5099 (25–200μM), and a concentration that could specifically inhibit MPC has not been defined so far [10, 12, 13, 14]. Several studies reported that doses of UK5099 on the order of 50 to 200μM UK5099 could suppress inflammatory cytokine production [10, 12, 13], leding to the conclusion that mitochondrial entry of pyruvate produced from enhanced glycolysis is critical for the activation of macrophages by LPS. In the current study, by using mice with genetic depletion of *Mpc*, we found that the inhibition of inflammatory cytokine production in LPS-stimulated macrophages by UK5099 is independent of MPC but shows concentration dependency. Selective MPC inhibitory effects of UK5099 are seen only in a narrow, low-dose range (< 10μM). Thus, conclusions drawn from studies on mitochondrial pyruvate transfer using higher doses of UK5099 than this should be evaluated carefully.

Excessive UK5099 impairs OXPHOS and HIF-1α stabilization

Although UK5099 suppresses the inflammatory responses of LPS stimulated macrophages due to its off-target effects rather than MPC inhibition, elucidating its true targets and mechanism of action is important to identify new compounds to treat inflammatory diseases. UK5099 at high concentrations (e.g 100 μM) effectively inhibits the production of key proinflammatory cytokines, including TNF-α, IL-6 and IL-12, suggesting that appropriate structural modification of this drug could be a promising strategy to curb excessive inflammatory responses. Of note, we found that UK5099 at high concentrations not only reduces the transportation of glucose-derived pyruvate into the TCA cycle but also suppresses the oxidation of other substrates, such as glutamate. As the transportation and metabolism of glutamate is independent of MPC, the inhibition of glutamate oxidation is at least one of the off-target effects of UK5099. On the other hand, it is unknown whether MPC inhibition is required in combination with the off targets of UK5099 to suppress inflammatory responses. Although MPC inhibition alone is unable to

reduce proinflammatory cytokines production in LPS stimulated macrophages, it is possible that it further decreases available substrates for OXPHOS when glutamate oxidation is impaired by high concentrations of UK5099. Further studies are required to investigate how macrophages precisely control metabolic reprogramming in mitochondria to fine tune inflammatory responses.

In conclusion, we found that MPC-mediated metabolism is dispensable for the activation of LPS stimulated macrophages. UK5099 inhibits the inflammatory response in macrophages, but this is due to its off-target effects rather than MPC inhibition.

Declarations

ACKNOWLEDGMENTS

This study was supported by the National Natural Science Foundation of China (81970073, 82170090), the Shanghai Science and Technology Commission (19ZR1441600), the Shanghai Pujiang Program (2020PJD051), the Outstanding Clinical Discipline Project of Shanghai Pudong (PWYgy2018-6) and the Academic Leaders Training Program of Pudong Health and Family Planning Commission of Shanghai (PWRd2019-02).

AUTHOR CONTRIBUTIONS

Conceptualization, F.W. and S.Z.; Methodology, F.W., S.Z., R.J., J.Z., H.G., and J.H.; Validation, F.W. and S.Z.; Investigation, L.R., S.Z., and P.Z.; Writing – Original Draft, F.W. and J.H.; Writing – Review & Editing, F.W., S.Z., Q.L., and J.H.; Supervision, F.W., Q.L., and J.H.; Funding Acquisition, F.W., Q.L., and J.H.

DECLARATION OF INTERESTS

The authors declare no competing interests.

References

1. O'Neill, L. A., Kishton, R. J., & Rathmell, J. (2016). A guide to immunometabolism for immunologists. Nature Reviews Immunology, 16(9), 553.

2. Wang, A., Luan, H. H., & Medzhitov, R. (2019). An evolutionary perspective on immunometabolism. Science, 363(6423).

3. Van den Bossche, J., O'Neill, L. A., & Menon, D. (2017). Macrophage immunometabolism: where are we (going)?. Trends in immunology, 38(6), 395-406.

4. Russell, D. G., Huang, L., & VanderVen, B. C. (2019). Immunometabolism at the interface between macrophages and pathogens. Nature Reviews Immunology, 19(5), 291-304.

5. Ryan, D. G., & O'Neill, L. A. (2020). Krebs cycle reborn in macrophage immunometabolism. Annual review of immunology, 38, 289-313.

6. Tannahill, G. M., Curtis, A. M., Adamik, J., Palsson-McDermott, E. M., McGettrick, A. F., Goel, G., ... & O'Neill, L. A. J. (2013). Succinate is an inflammatory signal that induces IL-1β through HIF-1α. Nature, 496(7444), 238-242.

7. Mills, E. L., Kelly, B., Logan, A., Costa, A. S., Varma, M., Bryant, C. E., ... & O'Neill, L. A. (2016). Succinate dehydrogenase supports metabolic repurposing of mitochondria to drive inflammatory macrophages. Cell, 167(2), 457-470.

8. Bricker, D. K., Taylor, E. B., Schell, J. C., Orsak, T., Boutron, A., Chen, Y. C., ... & Rutter, J. (2012). A mitochondrial pyruvate carrier required for pyruvate uptake in yeast, Drosophila, and humans. Science, 337(6090), 96-100.

9. Herzig, S., Raemy, E., Montessuit, S., Veuthey, J. L., Zamboni, N., Westermann, B., ... & Martinou, J. C. (2012). Identification and functional expression of the mitochondrial pyruvate carrier. Science, 337(6090), 93-96.

10. Lauterbach, M. A., Hanke, J. E., Serefidou, M., Mangan, M. S., Kolbe, C. C., Hess, T., ... & Latz, E. (2019). Toll-like receptor signaling rewires macrophage metabolism and promotes histone acetylation via ATP-citrate lyase. Immunity, 51(6), 997-1011.

11. Langston, P. K., Nambu, A., Jung, J., Shibata, M., Aksoylar, H. I., Lei, J., ... & Horng, T. (2019). Glycerol phosphate shuttle enzyme GPD2 regulates macrophage inflammatory responses. Nature immunology, 20(9), 1186-1195.

12. Meiser, J., Krämer, L., Sapcariu, S. C., Battello, N., Ghelfi, J., D'Herouel, A. F., ... & Hiller, K. (2016). Pro-inflammatory macrophages sustain pyruvate oxidation through pyruvate dehydrogenase for the synthesis of itaconate and to enable cytokine expression. Journal of Biological Chemistry, 291(8), 3932-3946.

13. Bae, S., Park, P. S. U., Lee, Y., Mun, S. H., Giannopoulou, E., Fujii, T., ... & Park-Min, K. H. (2021). MYC-mediated early glycolysis negatively regulates proinflammatory responses by controlling IRF4 in inflammatory macrophages. Cell Reports, 35(11), 109264.

14. Martínez-Reyes, I., Diebold, L. P., Kong, H., Schieber, M., Huang, H., Hensley, C. T., ... & Chandel, N. S. (2016). TCA cycle and mitochondrial membrane potential are necessary for diverse biological functions. Molecular cell, 61(2), 199-209.

15. Hill, B. G., Benavides, G. A., Lancaster, J. R., Ballinger, S., Dell'Italia, L., Zhang, J., & Darley-Usmar, V. M. (2012). Integration of cellular bioenergetics with mitochondrial quality control and autophagy. Biological chemistry, 393(12), 1485-1512.

16. Chua, Y. L., Dufour, E., Dassa, E. P., Rustin, P., Jacobs, H. T., Taylor, C. T., & Hagen, T. (2010). Stabilization of hypoxia-inducible factor-1α protein in hypoxia occurs independently of mitochondrial reactive oxygen species production. Journal of Biological Chemistry, 285(41), 31277-31284.

17. Agani, F. H., Pichiule, P., Chavez, J. C., & LaManna, J. C. (2002). Inhibitors of mitochondrial complex I attenuate the accumulation of hypoxia-inducible factor-1 during hypoxia in Hep3B cells. Comparative Biochemistry and Physiology Part A: Molecular & Integrative Physiology, 132(1), 107-109.

18. Cramer, T., Yamanishi, Y., Clausen, B. E., Förster, I., Pawlinski, R., Mackman, N., ... & Johnson, R. S. (2003). HIF-1α is essential for myeloid cell-mediated inflammation. Cell, 112(5), 645-657.

19. Ke, Q., & Costa, M. (2006). Hypoxia-inducible factor-1 (HIF-1). Molecular pharmacology, 70(5), 1469-1480.

20. McCommis, K. S., Chen, Z., Fu, X., McDonald, W. G., Colca, J. R., Kletzien, R. F., ... & Finck, B. N. (2015). Loss of mitochondrial pyruvate carrier 2 in the liver leads to defects in gluconeogenesis and compensation via pyruvate-alanine cycling. Cell metabolism, 22(4), 682-694.

21. Divakaruni, A. S., Paradyse, A., Ferrick, D. A., Murphy, A. N., & Jastroch, M. (2014). Analysis and interpretation of microplate-based oxygen consumption and pH data. Methods in enzymology, 547, 309-354.16. Vigueira, P. A., McCommis, K. S., Schweitzer, G. G., Remedi, M. S., Chambers, K. T., Fu, X., ... & Finck, B. N. (2014). Mitochondrial pyruvate carrier 2 hypomorphism in mice leads to defects in glucose-stimulated insulin secretion. Cell reports, 7(6), 2042-2053.

22. Divakaruni, A. S., Wiley, S. E., Rogers, G. W., Andreyev, A. Y., Petrosyan, S., Loviscach, M., ... & Murphy, A. N. (2013). Thiazolidinediones are acute, specific inhibitors of the mitochondrial pyruvate carrier. Proceedings of the national academy of sciences, 110(14), 5422-5427.

23. Divakaruni, A. S., Hsieh, W. Y., Minarrieta, L., Duong, T. N., Kim, K. K., Desousa, B. R., ... & Murphy, A. N. (2018). Etomoxir inhibits macrophage polarization by disrupting CoA homeostasis. Cell metabolism, 28(3), 490-503.

24. Lagziel, S., Gottlieb, E., & Shlomi, T. (2020). Mind your media. Nature Metabolism, 2(12), 1369-1372.

25. Gautier, E. L., Ivanov, S., Williams, J. W., Huang, S. C. C., Marcelin, G., Fairfax, K., ... & Randolph, G. J. (2014). Gata6 regulates aspartoacylase expression in resident peritoneal macrophages and controls their survival. Journal of Experimental Medicine, 211(8), 1525-1531.

26. Baardman, J., Verberk, S. G., van der Velden, S., Gijbels, M. J., van Roomen, C. P., Sluimer, J. C., ... & Van den Bossche, J. (2020). Macrophage ATP citrate lyase deficiency stabilizes atherosclerotic plaques.

Nature communications, 11(1), 1-15.

27. Wang, Y., Tang, B., Long, L., Luo, P., Xiang, W., Li, X., ... & Shi, C. (2021). Improvement of obesity-associated disorders by a small-molecule drug targeting mitochondria of adipose tissue macrophages. Nature communications, 12(1), 1-16.

28. Liu, X., Cooper, D. E., Cluntun, A. A., Warmoes, M. O., Zhao, S., Reid, M. A., ... & Locasale, J. W. (2018). Acetate production from glucose and coupling to mitochondrial metabolism in mammals. Cell, 175(2), 502-513.

29. Bensard, C. L., Wisidagama, D. R., Olson, K. A., Berg, J. A., Krah, N. M., Schell, J. C., ... & Rutter, J. (2020). Regulation of tumor initiation by the mitochondrial pyruvate carrier. Cell metabolism, 31(2), 284-300.

30. Vacanti, N. M., Divakaruni, A. S., Green, C. R., Parker, S. J., Henry, R. R., Ciaraldi, T. P., ... & Metallo, C. M. (2014). Regulation of substrate utilization by the mitochondrial pyruvate carrier. Molecular cell, 56(3), 425-435.

31. Bender, T., Pena, G., & Martinou, J. C. (2015). Regulation of mitochondrial pyruvate uptake by alternative pyruvate carrier complexes. The EMBO journal, 34(7), 911-924.

32. Schell, J. C., & Rutter, J. (2013). The long and winding road to the mitochondrial pyruvate carrier. Cancer & metabolism, 1(1), 1-9.

33. Proudlove, M. O., Beechey, R. B., & Moore, A. L. (1987). Pyruvate transport by thermogenic-tissue mitochondria. Biochemical Journal, 247(2), 441-447.

34. Halestrap, A. P. (1975). The mitochondrial pyruvate carrier. Kinetics and specificity for substrates and inhibitors. Biochemical Journal, 148(1), 85-96.

35. Zhang, X., Goncalves, R., & Mosser, D. M. (2008). The isolation and characterization of murine macrophages. Current protocols in immunology, 83(1), 14-1.

36. Wang, F., Zhang, S., Jeon, R., Vuckovic, I., Jiang, X., Lerman, A., ... & Herrmann, J. (2018). Interferon gamma induces reversible metabolic reprogramming of M1 macrophages to sustain cell viability and pro-inflammatory activity. EBioMedicine, 30, 303-316.

37. Wang, F., Zhang, S., Vuckovic, I., Jeon, R., Lerman, A., Folmes, C. D., ... & Herrmann, J. (2018). Glycolytic stimulation is not a requirement for M2 macrophage differentiation. Cell metabolism, 28(3), 463-475.

38. Lee WN, Byerley LO, Bergner EA, Edmond J. (1991). Mass isotopomer analysis: theoretical and practical considerations. Biol Mass Spectrom. 20, 451-8.

Methods

Mouse Strains

Mpc1$^{fl/fl}$ mice were generated by CRISPR/Cas9 which targets exon 3-5 of the *Mpc1* gene of mice in C57BL/6J background. *Mpc1*$^{fl/fl}$ mice were then crossed with Lyz2-Cre transgenic mice (The Jackson Laboratory) to generate mice with a myeloid-specific deletion of MPC1 (*Mpc1*$^{-/-}$). Female *Mpc1*$^{-/-}$ (6-8 weeks of age) and their littermate control mice (*Mpc1*$^{fl/fl}$) were used in this study. Wild-type bone marrow-derived macrophages (BMDMs) were isolated from female wild-type C57BL/6J mice (6-8 weeks of age). The mice were bred and maintained under pathogen-free conditions with ad libitum access to food and water. This study was approved by the Tongji University Institutional Animal Use and Care Committee (IACUC).

Bone Marrow Derived Macrophage Isolation

Bone marrow-derived macrophages (BMDMs) were isolated as previously described (35-37). Briefly, mice were individually euthanized by CO_2 inhalation, and both the femur and tibia were isolated and placed in PBS after removing the skin and muscle. Bone marrow cells were then flushed out from the bone, resuspended and grown in RPMI-1640 media (10% heat-inactivated FBS and 1% penicillin and streptomycin) containing 20 ng/ml M-CSF. Half the volume of fresh growth medium was added on day 4. After 7 days in culture, macrophages were harvested and plated for further experimentation.

Macrophage activation

BMDMs were seeded at 1×10^6/mL for experiments unless stated otherwise. The cells were activated with LPS (100 ng/mL) for the indicated times.

Metabolism assay

Extracellular acidification rate (ECAR) and oxygen consumption rate (OCR) of BMDMs were analyzed with an XF96 Extracellular Flux Analyzer (Agilent) as described (36, 37). Briefly, WT, *Mpc1*$^{fl/fl}$ or *Mpc1*$^{-/-}$ BMDMs were seeded in XF96 Cell Culture Microplates at 8×10^4 cells/well for 24 hours before the experiments. Cells were treated with and without different concentrations of UK5099 for 1 hour, followed by simulation with LPS for 4 hours or 24 hours. Cells were then switched to Seahorse media and ECAR and OCR were measured at baseline and after the injection of different inhibitors (Oligomycin, FCCP, Rotenone and Antimycin A).

To measure substrate specific respiration, BMDMs were permeabilized and provided with different oxidizable substrates (17, 18, 19). Briefly, *Mpc1*$^{fl/fl}$ and *Mpc1*$^{-/-}$ BMDMs were seeded in XF96 Cell Culture Microplates at 8×104 cells/well for 24 hours before the experiments. Cells were treated with or without different concentrations of UK5099 for 1 hour, followed by stimulation with LPS for 4 hours. Cells were then washed twice and switched to MAS buffer (70 mM sucrose, 220 mM mannitol, 10 mM KH_2PO_4, 5

mM $MgCl_2$, 2 mM HEPES, and 1 mM EGTA; pH 7.2) containing 1nM XF Plasma Membrane Permeabilizer (XF PMP, Agilent) to selectively permeabilize the plasma membrane. For pyruvate-dependent respiration, cells were provided with 5 mM pyruvate, 0.5 mM malate and 2 mM DCA; For glutamate-dependent respiration, cells were offered with 10 mM glutamate and 5 mM malate. ECAR and OCR were measured at baseline and after the injection of different inhibitors (Oligomycin, FCCP, Rotenone and Antimycin A).

Intracellular metabolites were measured by GC/MS (36, 37). Briefly, 2× 10^6 WT, *Mpc1*$^{fl/fl}$ or *Mpc1*$^{-/-}$ BMDMs were seeded in 35 mm petri dished for 24 hours. Cells were treated with or without different concentrations of UK5099 for 1 hour, followed by stimulation with LPS for 4 hours. After the removal of culture medium, cells were washed 3 times with ice-cold saline, quenched with -20℃ 1:1 water:methanol, and flash frozen by rapid immersion of dishes in liquid nitrogen. Frozen cells were scrapped off culture dishes kept on dry ice, frozen in liquid nitrogen and thawed on ice for 20 minutes. After vortexing, samples were centrifuged at 10,000 g for 10 minutes at 4 °C. The supernatant was then collected. The extraction procedure was repeated, followed by the supernatant combined and completely dried in a SpeedVac concentrator, methoximated using 10 µL of MOX™ Regent at 30°C for 90 min and then derivatized using 40 µL of MSTFA+1% TMCS (N-methyl-N-trimethylsilyltrifluoroacetamide with 1% trimethylchlorosilane) at 37°C for 30 min. Metabolite levels were determined using GC-MS (Hewlett-Packard, HP 5980B) with DB5-MS column. GC-MS spectra were deconvoluted using AMDIS software, then SpectConnect software was used to create the metabolite peaks matrix. The Agilent Fiehn GC/MS Metabolomics RTL Library was used for metabolite identification. Ion count peak area was used for analysis of the relative abundance of the metabolites.

Metabolite levels in the culture medium were analyzed by NMR spectroscopy to determine the consumption or the production of certain substrates (36, 37). Briefly, WT, *Mpc1*$^{fl/fl}$ or *Mpc1*$^{-/-}$ BMDMs were treated with or without different concentrations of UK5099 for 1 hour, followed by stimulation with LPS for 24 hours. Original and cell culture media were collected and deproteinized before NMR analysis. In 150 µL of media samples 450 µL of cold methanol were added. The samples were spun down at 10,000 g for 10 min, supernatants were collected and dried down in centrifugal vacuum evaporator for 12 h. To dried samples, 500 µL of 0.1 M phosphate buffer and 50 µL of 1 mM TSP-d_4 solution in D_2O were added. Samples were vortexed for 20 seconds and transferred to 5 mm NMR tubes. NMR spectra were acquired on a Bruker 500 MHz Avance III HD spectrometer equipped with a BBO cryoprobe and SampleCase auto sampler (Bruker Biospin, Rheinstetten, Germany). ^{1}H-NMR spectra were recorded using 1D noesy pulse sequence with presaturation (noesygppr1d), with 90 degree pulse (~13 µs), 4.68 seconds acquisition time, and 4 seconds relaxation delay. Spectra were phase and baseline corrected using the Topspin 3.5 software. Metabolites were identified and quantified using the software program Chenomx NMR Suite 8.2, by fitting the spectral lines of library compounds into the recorded NMR spectrum of the cell extracts. The quantification was based on peak area of TSP-d_4 signal, and metabolite concentrations were reported as µM in medium.

$^{13}C_6$-glucose and $^{13}C_5$-glutamine tracing experiments

Metabolic tracing analysis of U-[^{13}C]-glucose, U-[^{13}C]-glutamine and 2-^{13}C-pyruvate in BMDMs was determined by GC/MS. Briefly, 6×10^6 cells were incubated in RPMI-1640 medium containing 11.1 mM $^{13}C_6$-glucose, 2 mM $^{13}C_5$-glutamine or 1 mM 2-^{13}C-pyruvate. Cells were treated with or without different concentrations of UK5099 for 1 hour, followed by stimulation with LPS for 4 hours. Samples were collected and processed as described for intracellular metabolite measurement. Metabolites were quantified based on total ion count peak area of specific mass ions. To determine ^{13}C-labeling, mass information for known fragments of labeled metabolites was retrieved. These fragments contained either the whole or partial carbon skeleton of the metabolite. For each fragment, the retrieved data comprised mass intensities for the lightest isotopomer (without any heavy isotopes, M+0), and isotopomers with increasing unit mass (up to M+6) relative to M0. These mass distributions were normalized by dividing by the sum of M0 to M6, and corrected for the natural abundance of heavy isotopes, using matrix-based probabilistic methods as described (38) implemented in Microsoft Excel. ^{13}C-labeling data are expressed as fractional abundance of each isotopologue of a measured metabolite pool, or relevant enrichment of each metabolite. Data were from three biological replicates.

Nucleotide measurements

Intracellular nucleotides were measured by HPLC (37). WT, *Mpc1*$^{fl/fl}$ or *Mpc1*$^{-/-}$ BMDMs were plated at 0.5×10^6 cells/ml in 35 mm Corning Dishes for 24 hours. Cells were then treated with or without different concentrations of UK5099 for 1 hour and subsequently stimulated with LPS for 4 hours. After culture medium was removed, cells were quickly rinsed with PBS, quenched with 6% ice-cold $HClO_4$, and flash frozen by rapid immersion of dishes in liquid nitrogen. The cells were stored at −80° C prior to nucleotide analysis. Frozen cells were scrapped off culture dishes kept on dry ice and transferred to a micro-centrifuge tube chilled in liquid nitrogen. The frozen cells were homogenized using a Kimble® homogenizer (SIGMA, St. Louis, MO) in 200 µL ice cold 0.6 N perchloric acid to extract the nucleotides. The homogenate was centrifuged at 10,000 g for 10 min at 4° C. The supernatant was collected and neutralized to pH 7.4 with 2 M KHCO3 (100:35, by v/v). After centrifuging at 10,000 g for 10 minutes at 4 °C, nucleotides in the supernatant were separated on a reverse-phase Discovery C18 column (SIGMA, St. Louis, MO) with the Agilent 1290 HPLC system (Agilent, Santa Clara, CA), as described previously (37). Briefly, a phosphate buffer with tetrabutylammonium sulfate and methanol mixture was used as mobile phase at 0.7 ml/min flow rate. Gradient elution was applied and the separation of nucleotides was completed in 10 minutes. The nucleotide levels were normalized by cell number.

Mitochondrial membrane potential measurement

Cells were plated at 0.5×10^6 cells/ml in 12-well plates and treated with different concentrations of UK5099 for 1 hour, followed by stimulation with LPS for 4 hours. After removing culture media, cells were washed and incubated in PBS containing 50nM Mito Tracker Red (Thermo Fisher Scientific) at 37°C in the dark for 30 min. After 3 washes, cells were then collected in 500 µl PBS by using a cell scraper and transferred to polypropylene FACS tubes. Aqua fluorescent reactive dye (Thermo Fisher Scientific) was

applied to excluded dead cells. Cells were then analyzed using a LSRFortessa flow cytometer, and data were analyzed using FlowJo software.

Gene expression analysis by 3' RNA sequencing

Mpc1$^{fl/fl}$ and *Mpc1*$^{-/-}$ BMDMs were seeded in 12 well plates (1*10^6/well) and stimulated with or without LPS for 4 h after pretreatment with UK5099 (100μM) or DMSO for 1 h. After washing with PBS, cells were collected in Trizol (Thermo Fisher Scientific) and stored in liquid nitrogen. RNA was extracted and a total amount of 1 μg RNA per sample was used as input material for the RNA sample preparations. Briefly, mRNA was purified from total RNA using poly-T oligo-attached magnetic beads. Fragmentation was carried out using divalent cations under elevated temperature and the library fragments were purified with AMPure XP system (Beckman Coulter, Beverly, USA). Next, PCR was performed with Phusion High-Fidelity DNA polymerase, Universal PCR primers and Index (X) Primer. Lastly, PCR products were purified (AMPure XP system) and library quality was assessed on the Agilent Bioanalyzer 2100 system. The clustering of the index-coded samples was performed on a cBot Cluster Generation System using TruSeq PE Cluster Kit v3-cBot-HS (Illumina) according to the manufacturer's instructions. After cluster generation, the library preparations were sequenced on an Illumina Novaseq platform, and 150 bp paired-end reads were generated.

Western blotting

After different treatment and stimulation, cells were lysed in RIPA buffer containing Complete Mini EDTA-Free protease inhibitor cocktail and phosphatase inhibitor cocktail (Roche). Protein concentrations of cell lysate were measured by Pierce BCA protein assay kit (Thermo Fisher Scientific) and equal amount of protein from different samples were used. Cell lysate was then boiled in SDS sample buffer for 5 mins at 95-100 °C, separated by SDS-PAGE, and transferred to PVDF membranes (Bio-Rad). The membranes were blocked in TBS plus 5% nonfat dry milk (Bio-Rad) for 1 hour and then incubated with primary antibodies overnight at 4 °C. After three washes, the membranes were incubated with HRP-linked secondary antibodies for 1 hour at room temperature in TBS-T plus 5% nonfat dry milk. ECL western blotting chemiluminescent substrates (Thermo Fisher Scientific) were added for 5 min after washing three times. Bands of interest were developed by using an autoradiographic film.

ELISA

Cells were seeded in 24 well plates (5×10^5/well) and treated with different reagents before stimulation with or without LPS for the indicated times. The supernatants were collected and stored at -80 °C for further measurements. Concentrations of cytokines in supernatants were determined by ELISA kits (R&D systems) according to the manufacturer's instructions.

Quantitative real-time PCR

Cells were seeded in 24 well plates (5×10^5/well) and treated with different reagents before stimulation with or without LPS for indicated time. Total RNA was extracted by using RNeasy Plus Mini Kit with DNase treatment (QIAGEN). Equal amounts of RNA from different samples were reversely transcribed into cDNA using the RevertAid First Strand cDNA Synthesis Kit with random hexamer primer (Thermo Fisher Scientific). Quantitative real-time PCR was performed using the PowerUp™ SYBR™ Green Master Mix (Thermo Fisher Scientific) on a QuantStudio 6 Flex System (Applied Biosystems). Gene expression levels were normalized to the housekeeping gene GAPDH. The primer sequences used for gene expression analysis were listed in Supplementary Table 1.

Cell viability

Cell viability was tested by the XTT assay (Cell Signaling Technology). Briefly, 1×10^5 /well of BMDMs were seeded in 96-well plates and treated with different reagents before stimulation with or without LPS for the indicated times. Each well was added with 50 μl XTT detection solution and absorbance was read at 450 nm after incubation at 37^{o}C for 3h.

Endotoxin-Induced Model of Sepsis

Male and female mice aged between 10 and 12 weeks were used for in vivo LPS challenge experiment. Briefly, sex- and age-matched *Mpc1*$^{fl/fl}$ and *Mpc1*$^{-/-}$mice were randomly assigned to the vehicle control and LPS groups. Mice were peritoneally injected with LPS (15mg/kg) to induce an endotoxemia model. Serum and peritoneal lavage fluid (PLF) samples were collected at 6 hours after injection. Proinflammatory cytokine levels in serum and PLF were determined by ELISA.

Flow cytometry

After collection from endotoxemia mice models, peritoneal cells were centrifuged and resuspended in PBS containing 1% BSA and 1mM EDTA. Cells were incubated with the anti-mouse CD16/32 for 10 min at room temperature to block FC receptors and then stained with CD45, F4/80, CD11b and CD86 antibodies on ice for 20 min in the dark. After two times washing, cells were assayed by an Arial II-Optics flow cytometer and data were analyzed using the FlowJo 10.0 software. Peritoneal macrophages were gated as CD45^{+}CD11b^{+}F4/80^{+} and CD86 expression were compared between Mpc1$^{fl/fl}$ and Mpc1$^{-/-}$mice.

Statistical Analysis

Results were presented as mean ± standard error of the mean (sem). The unpaired Student's t-test was used to test the differences between two groups, based on the assessment of variance of the data. All data were analyzed by GraphPad Prism software (version 7). * $p<0.05$, ** $p<0.01$, *** $p<0.001$, **** $p<0.0001$. Detailed statistical values are provided in the figure legends.

DATA AND CODE AVAILABLE

The raw RNA sequencing data files reported in this study is uploading to NCBI and will be ready for access at any stage during the submission.

Figures

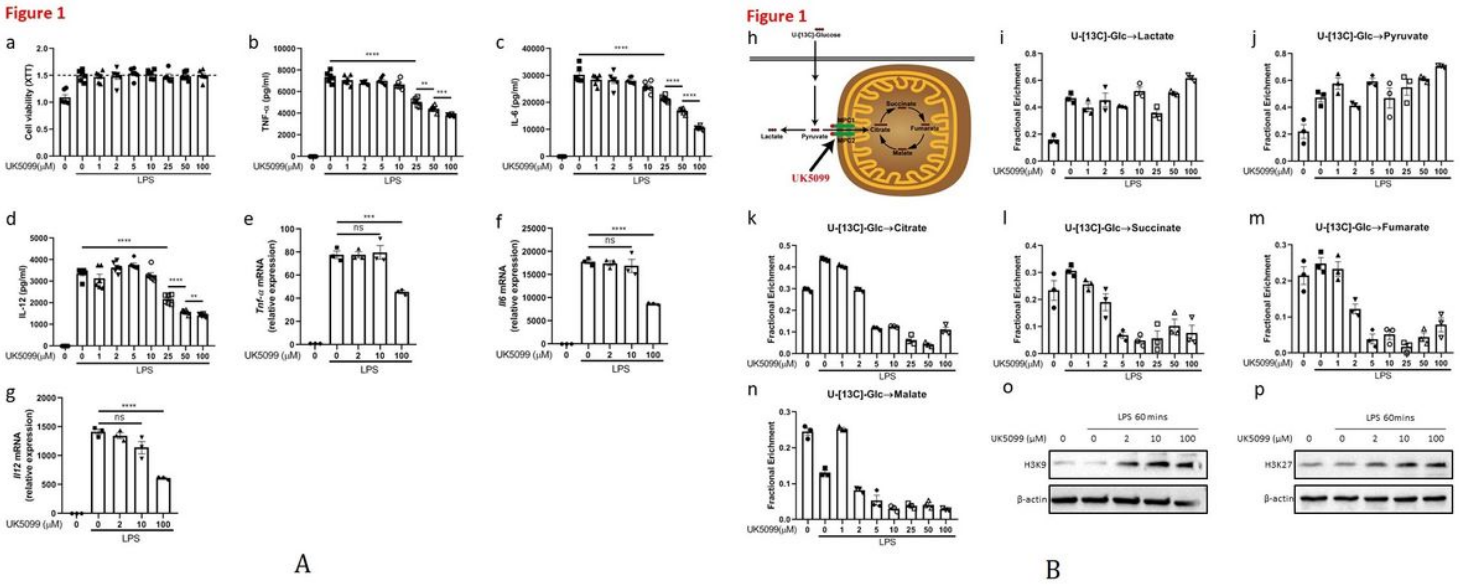

Figure 1

UK5099 Suppressed Inflammatory Cytokines Production Is Concentration Dependent

(a) Cell viability of WT BMDMs after 24 hours stimulation with LPS ± 1 hour pre-treatment with different concentrations of UK5099. Data are representative of three independent experiments (n = 6, mean ± SEM).

(b) to (d) Proinflammatory cytokines secretion of WT BMDMs after 24 hours stimulation with LPS ± 1 hour pre-treatment with different concentrations of UK5099. **p < 0.01, ***p < 0.001, ****p < 0.0001. Data are representative of three independent experiments (n = 6, mean ± SEM).

(e) to (g) Expression of proinflammatory cytokines mRNA in WT BMDMs after 4 hours stimulation with LPS ± 1 hour pre-treatment with different concentrations of UK5099. ***p < 0.001, ****p < 0.0001; ns, no significant difference. Data are representative of three independent experiments (n = 3, mean ± SEM).

(h) to (n) U-[^{13}C]-Glucose labeled glycolytic metabolites (i and j) and TCA cycle metabolites (k to n) in WT BMDMs after 4 hours stimulation with LPS ± 1 hour pre-treatment with different concentrations of UK5099. Data are representative of three independent experiments (n = 3, mean ± SEM).

(o) to (p) Immunoblot analysis of histone acetylation (H3K9 and H3K27) in WT BMDMs after 1 hour stimulation with LPS ± 1 hour pre-treatment with different concentrations of UK5099. Data are

representative of three independent experiments.

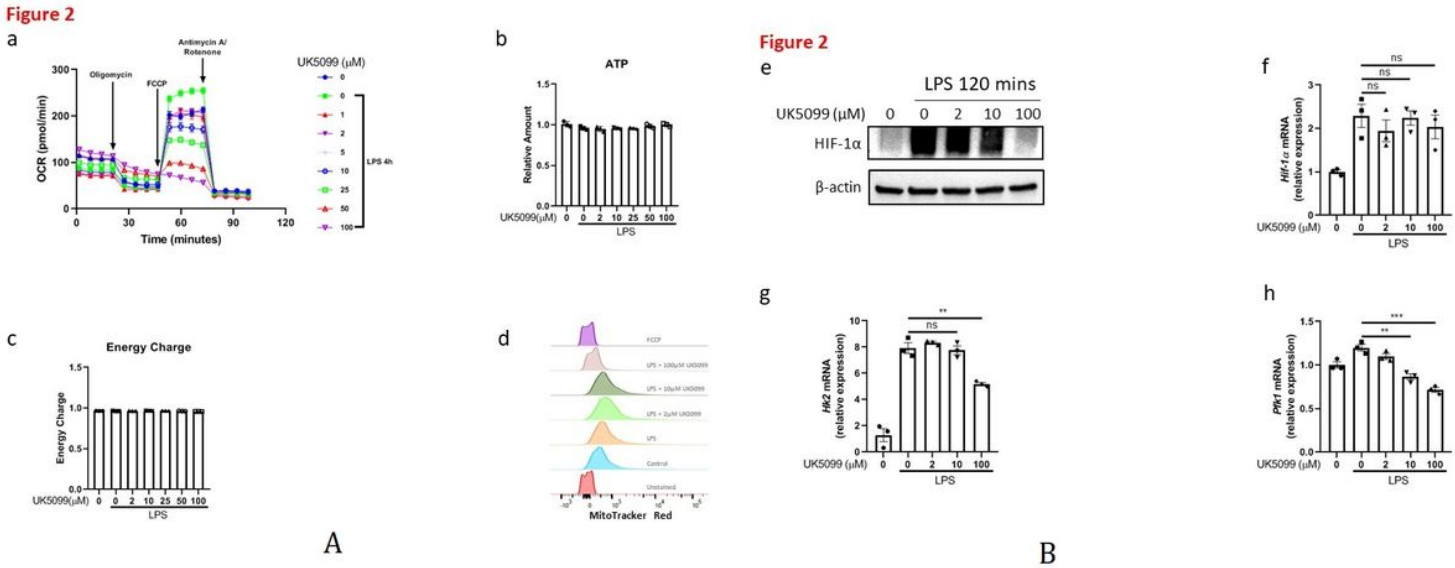

Figure 2

UK5099 Suppresses Oxidative Phosphorylation (OXPHOS), Mitochondrial Membrane Potential as well as HIF-1α Stabilization and Its Regulation of Genes Expression

(a) OCR of WT BMDMs after 4 hours stimulation with LPS ± 1 hour pre-treatment with different concentrations of UK5099. The arrows indicate injection of the activator. Data are representative of three independent experiments (n = 8, mean ± SEM).

(b) to (c) ATP production (b) and energy charge (c) of WT BMDMs after 4 hours stimulation with LPS ± 1 hour pre-treatment with different concentrations of UK5099. Data are representative of three independent experiments (n = 5, mean ± SEM).

(d) Flow cytometry analysis of mitochondrial membrane potential in WT BMDMs after 4 hours stimulation with LPS ± 1 hour pre-treatment with different concentrations of UK5099. Data are representative of three independent experiments.

(e) Immunoblot analysis of HIF-1α expression in WT BMDMs after 2 hours stimulation with LPS ± 1 hour pre-treatment with different concentrations of UK5099. Data are representative of three independent experiments.

(f) Expression of *Hif-1α* mRNA in WT BMDMs after 2 hours stimulation with LPS ± 1 hour pre-treatment with different concentrations of UK5099. ns, no significant difference. Data are representative of three independent experiments.

(g) to (h) Expression of *Hk2* and *Pfk1* mRNA in WT BMDMs after 4 hours stimulation with LPS ± 1 hour pre-treatment with different concentrations of UK5099. **p < 0.01, ***p < 0.001; ns, no significant

difference. Data are representative of three independent experiments (n = 3, mean ± SEM).

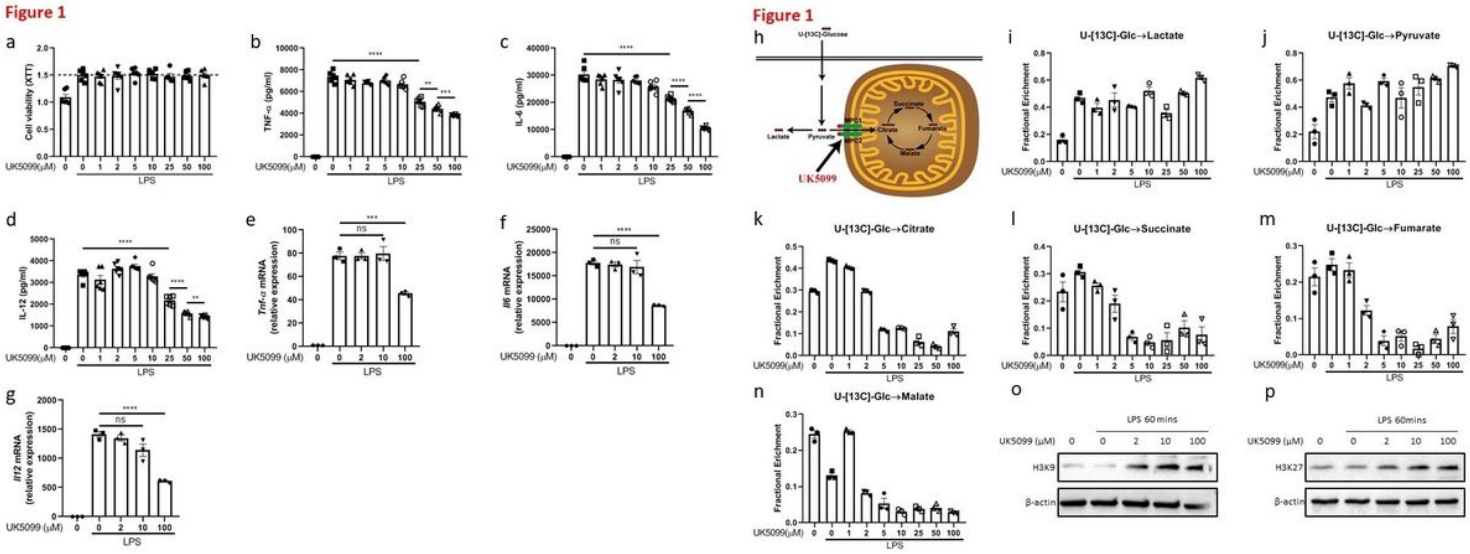

Figure 3

UK5099 Suppresses Inflammatory Responses Independent of MPC Expression

(a) Gene targeting strategy for *Mpc1* depletion in exon 3-5 in a Lyz2-conditional manner.

(b) and (c) Expression of *Mpc1* and *Mpc2* mRNA in $Mpc^{fl/fl}$ and $Mpc^{-/-}$ BMDMs. ****p < 0.0001; ns, no significant difference. Data are representative of at least ten independent experiments (n = 4, mean ± SEM).

(d) and (e) Expression of MPC1 and MPC2 protein in $Mpc^{fl/fl}$ and $Mpc^{-/-}$ BMDMs. Data are representative of at least ten independent experiments.

(f) to (h) Expression of proinflammatory cytokines mRNA in $Mpc^{fl/fl}$ and $Mpc^{-/-}$ BMDMs after 4 hours stimulation with LPS ± 1 hour pre-treatment with UK5099 (100μM). **p < 0.01, ***p < 0.001. Data are representative of three independent experiments (n = 4, mean ± SEM).

(i) to (k) Proinflammatory cytokines secretion by $Mpc^{fl/fl}$ and $Mpc^{-/-}$ BMDMs after 24 hours stimulation with LPS ± 1 hour pre-treatment with UK5099 (100μM). *p < 0.05, ****p < 0.0001. Data are representative of three independent experiments (n = 4, mean ± SEM).

(l) Cell viability of $Mpc^{fl/fl}$ and $Mpc^{-/-}$ BMDMs after 24 hours stimulation with LPS ± 1 hour pre-treatment with UK5099 (100μM). ns, no significant difference. Data are representative of three independent experiments (n = 8, mean ± SEM).

(m) to (o) Volcano plots of gene expression in $Mpc^{fl/fl}$ and $Mpc^{-/-}$ BMDMs after 4 hours stimulation with LPS ± 1 hour pre-treatment with UK5099 (100μM).

(p) Heat map of gene expression in *Mpc*$^{fl/fl}$ and *Mpc*$^{-/-}$ BMDMs after 4 hours stimulation with LPS ± 1 hour pre-treatment with UK5099 (100μM).

(q) KEGG enrichment analysis of differentially expressed genes in *Mpc*$^{fl/fl}$ and *Mpc*$^{-/-}$ BMDMs after 4 hours stimulation with LPS ± 1 hour pre-treatment with UK5099 (100μM).

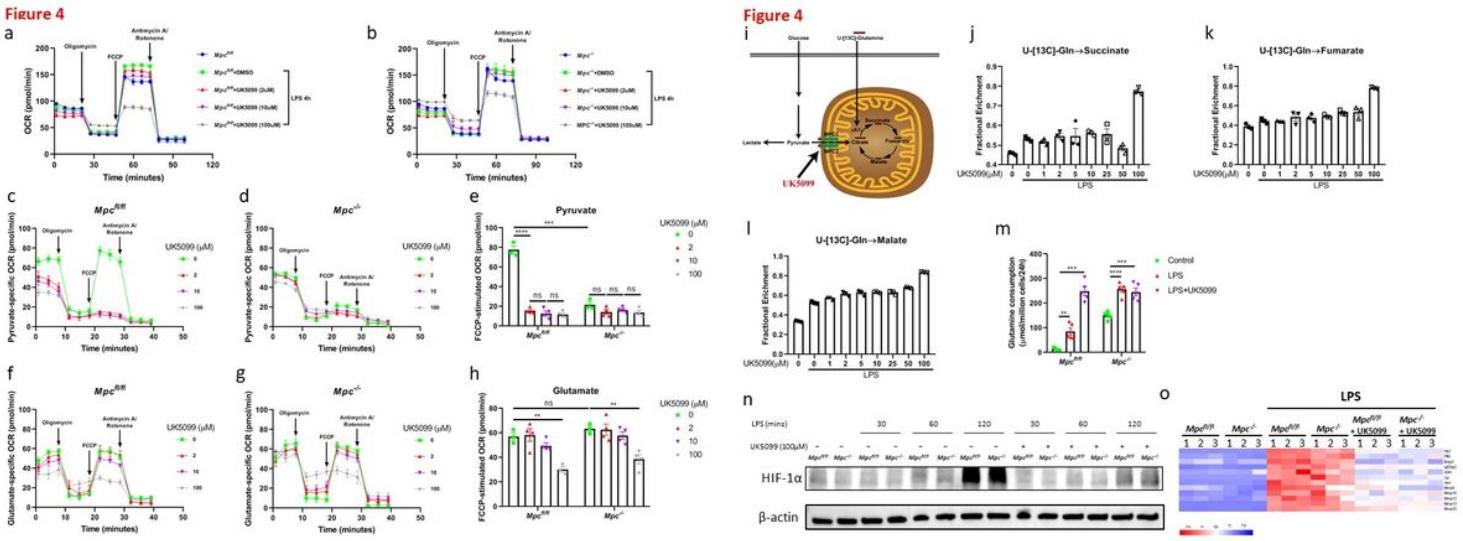

Figure 4

Off-Target Effects of UK5099 on Cellular Metabolism and HIF-1α Stabilization

(a) and (b) OCR of *Mpc*$^{fl/fl}$ (a) and *Mpc*$^{-/-}$ (b) BMDMs after 4 hours stimulation with LPS ± 1 hour pre-treatment with different concentrations of UK5099. The arrows indicate injection of the activator. Data are representative of three independent experiments (n = 8, mean ± SEM).

(c) to (e) *Mpc*$^{fl/fl}$ and *Mpc*$^{-/-}$ BMDMs were stimulated by LPS for 4 hours ± 1 hour pre-treatment with different concentrations of UK5099. The cells were then permeabilized in MAS buffer and provided with pyruvate (5mM)/malate (0.5mM), after which OCR was measured. Vertical line indicates initial injection of the activator. ***p < 0.001, ****p < 0.0001; ns, no significant difference. Data are representative of three independent experiments (n = 8, mean ± SEM).

(f) to (h) *Mpc*$^{fl/fl}$ and *Mpc*$^{-/-}$ BMDMs were stimulated by LPS for 4 hours ± 1 hour pre-treatment with different concentrations of UK5099. The cells were then permeabilized in MAS buffer and provided with glutamate (10mM)/malate (5mM), after which OCR was measured. The arrows indicate injection of the activator. **p < 0.01; ns, no significant difference. Data are representative of three independent experiments (n = 8, mean ± SEM).

(i) to (l) U-[^{13}C]-Glutamine labeled TCA cycle metabolites in WT BMDMs after 4 hours stimulation with LPS ± 1 hour pre-treatment with different concentrations of UK5099. Data are representative of three independent experiments (n = 3, mean ± SEM).

(m) Glutamine consumption of *Mpc*$^{fl/fl}$ and *Mpc*$^{-/-}$ BMDMs after 24 hours stimulation with LPS ± 1 hour pre-treatment with UK5099 (100μM). **p < 0.01, ***p < 0.001, ****p < 0.0001. Data are representative of three independent experiments (n = 5, mean ± SEM).

(n) Immunoblot analysis of HIF-1α expression in *Mpc*$^{fl/fl}$ and *Mpc*$^{-/-}$ BMDMs after stimulation with LPS for the indicated times ± 1 hour pre-treatment with UK5099 (100μM). Data are representative of three independent experiments.

(o) Heat map of HIF-1α targeted gene expression of *Mpc*$^{fl/fl}$ and *Mpc*$^{-/-}$ BMDMs after 4 hours stimulation with LPS ± 1 hour pre-treatment with UK5099 (100μM).

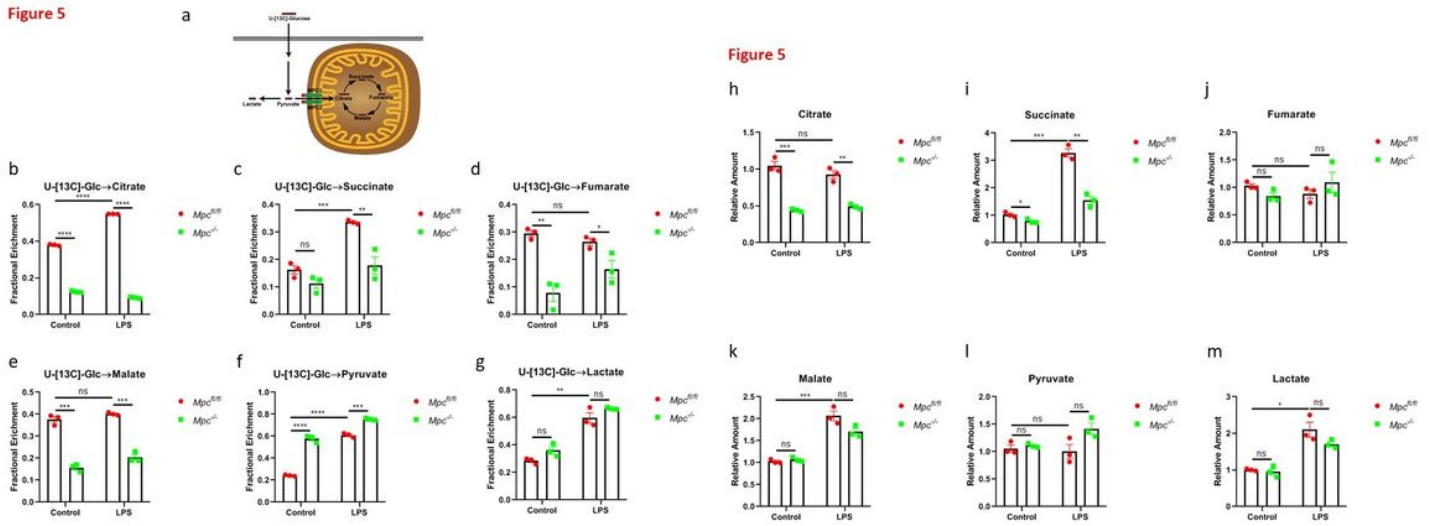

Figure 5

Mpc Depletion Reduces Glucose Fuel into TCA Cycle

(a) to (g) U-[^{13}C]-Glucose labeled TCA cycle metabolites (b to e) and glycolytic metabolites (f and g) in *Mpc*$^{fl/fl}$ and *Mpc*$^{-/-}$ BMDMs with or without stimulation by LPS for 4 hours. *p < 0.05, **p < 0.01, ***p < 0.001, ****p < 0.0001; ns, no significant difference. Data are representative of three independent experiments (n = 3, mean ± SEM).

(h) to (m) Total amount of TCA cycle metabolites (h to k) and glycolytic metabolites (l and m) in *Mpc*$^{fl/fl}$ and *Mpc*$^{-/-}$ BMDMs with or without stimulation by LPS for 4 hours. *p < 0.05, **p < 0.01, ***p < 0.001; ns, no significant difference. Data are representative of three independent experiments (n = 3, mean ± SEM).

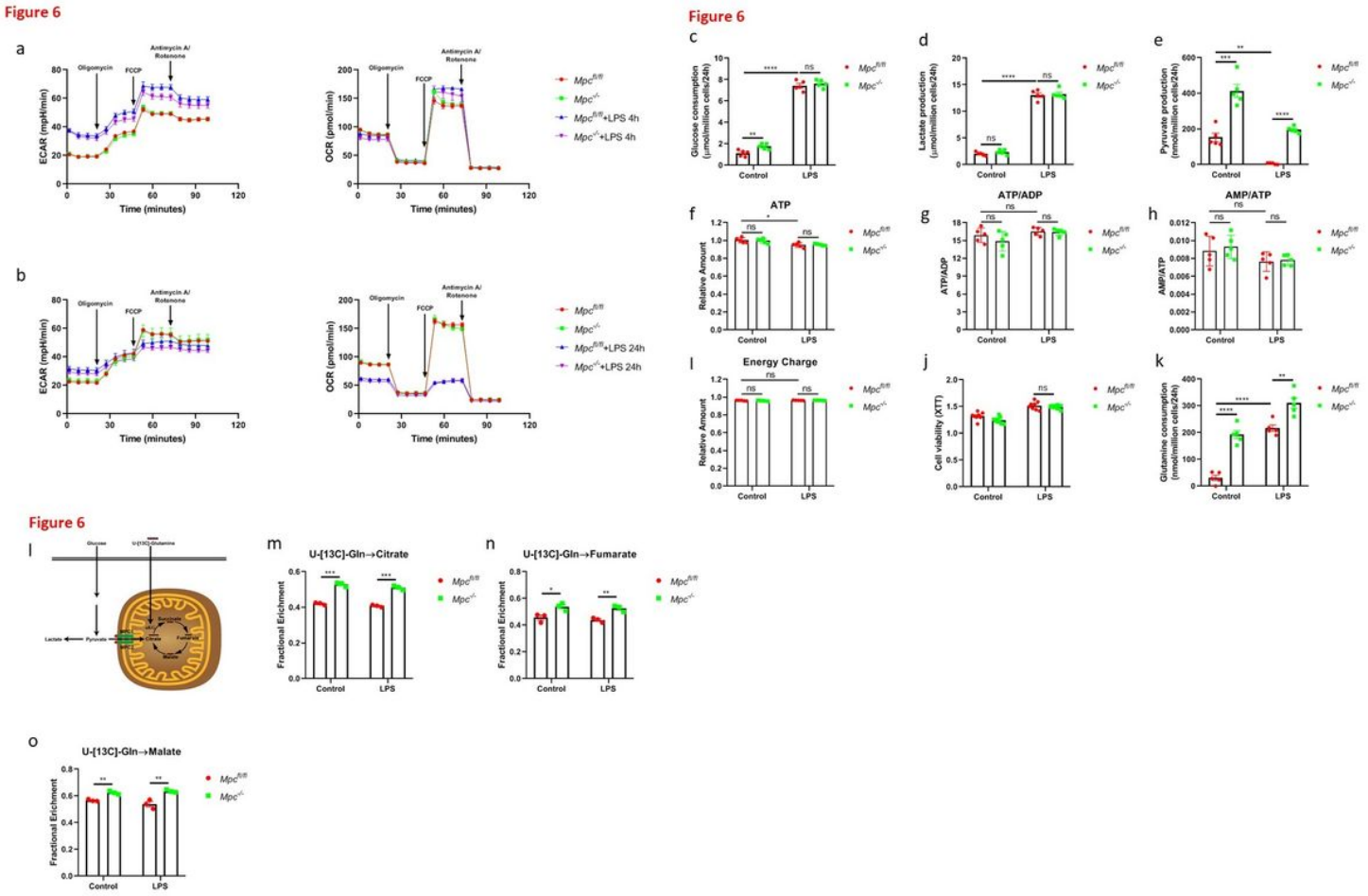

Figure 6

The Impacts of *Mpc* Depletion on Metabolic Reprogramming in LPS-stimulated Macrophages

(a) and (b) ECAR and OCR of $Mpc^{fl/fl}$ and $Mpc^{-/-}$ BMDMs left unstimulated (control) or stimulated with LPS for 4 hours (a) or 24 hours (b). The arrows indicate injection of the activator. Data are representative of three independent experiments (n = 6, mean ± SEM).

(c) to (e) Glucose consumption(c), lactate production(d) and pyruvate production (e) in $Mpc^{fl/fl}$ and $Mpc^{-/-}$ BMDMs left unstimulated (control) or stimulated with LPS for 24 hours. **p < 0.01, ***p < 0.001, ****p < 0.0001; ns, no significant difference. Data are representative of three independent experiments (n = 5, mean ± SEM).

(f) to (i) ATP, ATP/ADP, AMP/ATP and energy charge of $Mpc^{fl/fl}$ and $Mpc^{-/-}$ BMDMs left unstimulated (control) or stimulated with LPS for 2 hours. **p < 0.01; ns, no significant difference. Data are representative of three independent experiments (n = 5, mean ± SEM).

(j) Cell viability of $Mpc^{fl/fl}$ and $Mpc^{-/-}$ BMDMs with or without stimulation by LPS for 24 hours. ns, no significant difference. Data are representative of four independent experiments (n = 8, mean ± SEM).

(k) Glutamine consumption in *Mpc*$^{fl/fl}$ and *Mpc*$^{-/-}$ BMDMs with or without stimulation by LPS for 24 hours. **p < 0.01, ****p < 0.0001. Data are representative of three independent experiments (n = 5, mean ± SEM).

(l) to (o) U-[^{13}C]-Glutamine labeled TCA cycle metabolites in *Mpc*$^{fl/fl}$ and *Mpc*$^{-/-}$ BMDMs with or without stimulation by LPS for 4 hours. *p < 0.05, **p < 0.01, ***p < 0.001. Data are representative of three independent experiments (n = 3, mean ± SEM).

Figure 7

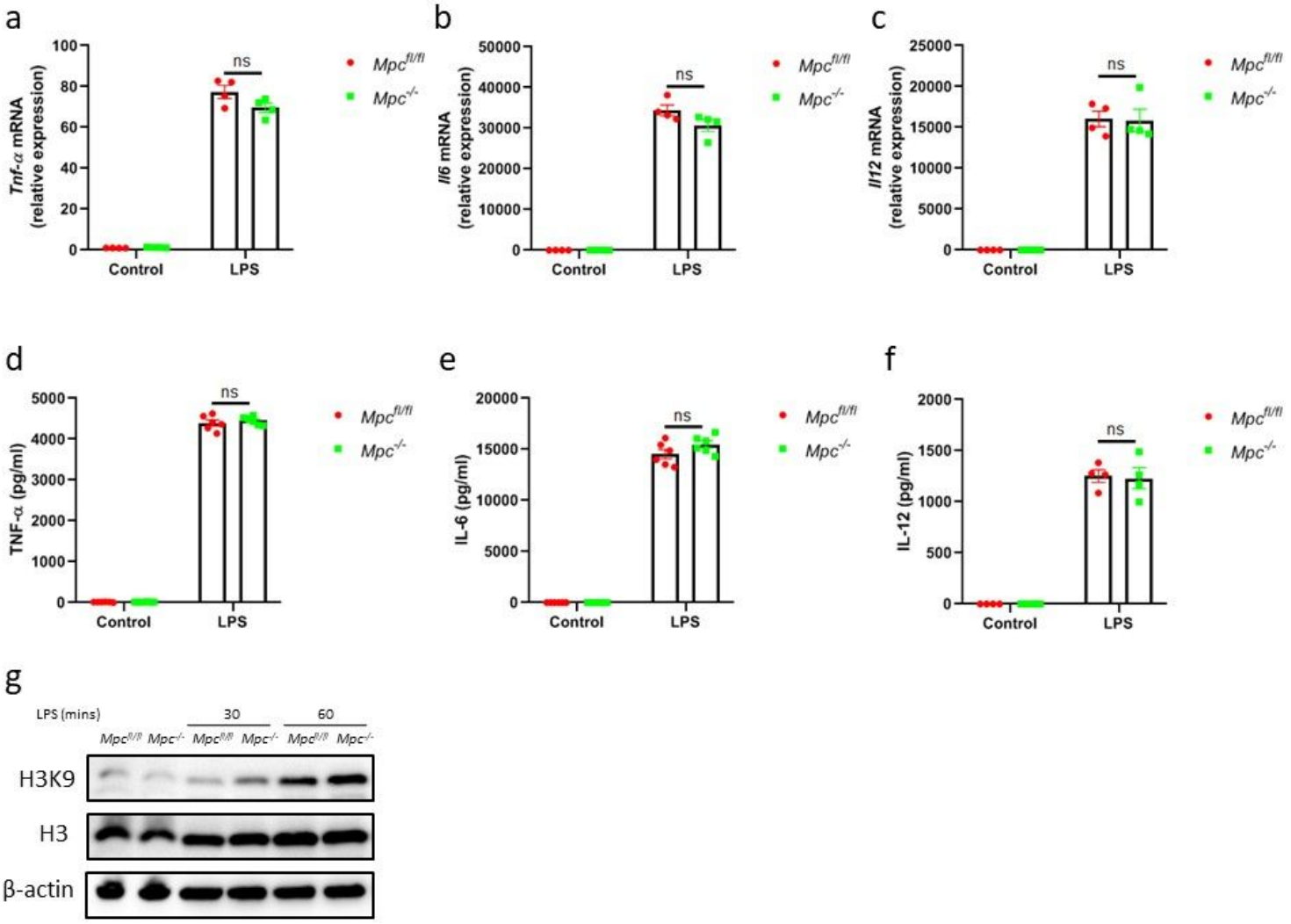

Figure 7

Mpc Depletion Is Dispensable for Proinflammatory Cytokines Production in LPS-stimulated Macrophages

(a) to (c) Expression of proinflammatory cytokines mRNA in *Mpc*$^{fl/fl}$ and *Mpc*$^{-/-}$ BMDMs with or without stimulation by LPS for 4 hours. ns, no significant difference. Data are representative of four independent experiments (n = 4, mean ± SEM).

(d) to (f) Proinflammatory cytokines secretion of *Mpc*$^{fl/fl}$ and *Mpc*$^{-/-}$ BMDMs with or without stimulation by LPS for 24 hours. ns, no significant difference. Data are representative of four independent

experiments (n = 6 for TNF-α and IL-6; n = 4 for IL-12; mean ± SEM).

(g) Immunoblot analysis of histone acetylation (H3K9) in *Mpc*$^{fl/fl}$ and *Mpc*$^{-/-}$ BMDMs with or without stimulation by LPS for the indicated times. Data are representative of five independent experiments.

Figure 8

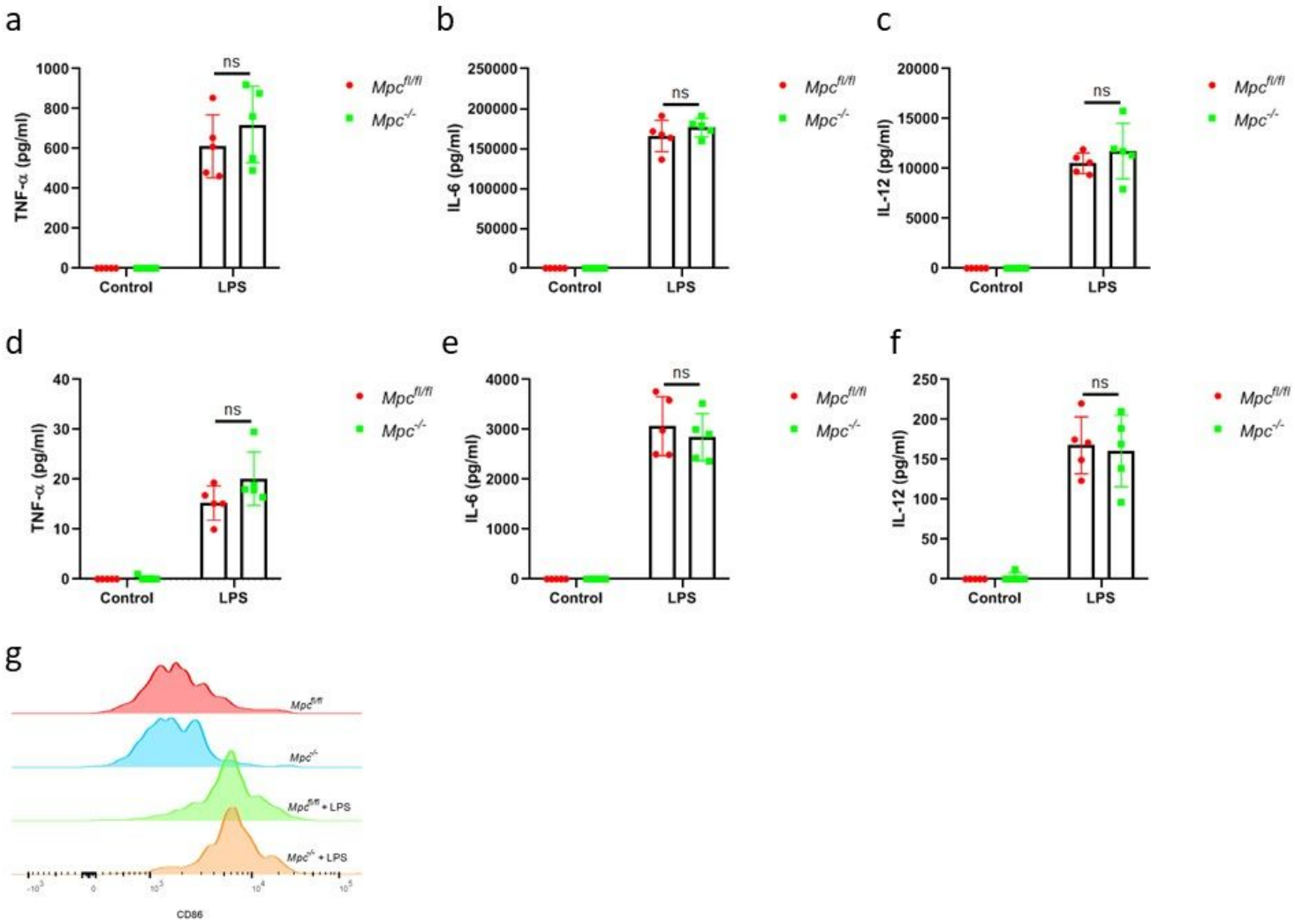

Figure 8

Mpc Is Not Required for Inflammatory Responses In Vivo

(a) to (c) Cytokine concentrations in serum of *Mpc*$^{fl/fl}$ and *Mpc*$^{-/-}$ mice with and without intraperitoneal injection of 15mg/kg LPS. ns, no significant difference. Data are representative of two independent experiments (n=5, mean ± SEM).

(d) to (f) Cytokine concentrations in peritoneal lavage of *Mpc*$^{fl/fl}$ and *Mpc*$^{-/-}$ mice with and without intraperitoneal injection of 15mg/kg LPS. ns, no significant difference. Data are representative of two independent experiments (n=5, mean ± SEM).

(g) CD86 surface expression on peritoneal macrophages of *Mpc*$^{fl/fl}$ and *Mpc*$^{-/-}$ mice with and without intraperitoneal injection of 15mg/kg LPS. Data are representative of three independent experiments.

Supplementary Files

This is a list of supplementary files associated with this preprint. Click to download.

- SupplementaryTable1.docx